Superconducting diode effect in selectively grown topological insulator based Josephson junctions

Gerrit Behner,* Abdur Rehman Jalil, Detlev Grützmacher, and Thomas Schäpers†
Peter Grünberg Institut (PGI-9), Forschungszentrum Jülich, 52425 Jülich, Germany
and JARA-Fundamentals of Future Information Technology, Jülich-Aachen Research Alliance,
Forschungszentrum Jülich and RWTH Aachen University, Germany

(Received 13 March 2025; revised 11 August 2025; accepted 22 October 2025; published 28 January 2026)

The Josephson diode effect, where the switching current magnitude depends on its direction, arises when both time-reversal and inversion symmetries are broken, often achieved by a combination of spin-orbit interaction and applied magnetic fields. Taking advantage of the strong spin-orbit coupling inherent in three-dimensional topological insulators, we study this phenomenon in Nb/$Bi_{0.8}Sb_{1.2}Te_3$/Nb Josephson weak-link junctions. Under an in-plane magnetic field perpendicular to the current direction, we observe a pronounced Josephson diode effect with efficiencies up to 7%. A crucial component of this behavior is the nonsinusoidal current-phase relationship and an anomalous phase shift, which we attribute to the presence of a ballistic supercurrent component due to the surface states. These findings open up new avenues for harnessing and controlling the Josephson diode effect in topological material systems.

DOI: 10.1103/gc7k-rn8q

I. INTRODUCTION

The superconducting diode effect, analogous to its classical semiconductor counterpart, refers to the nonreciprocal flow of dissipationless supercurrent in superconducting circuits [1,2]. Unlike conventional diodes, the superconducting diode effect can arise without requiring electron-hole asymmetry, for example, in Josephson junctions, thus being referred to as the Josephson diode effect (JDE). This effect is closely associated with a variety of exotic phenomena in unconventional superconducting systems and holds significant promise for transforming superconducting electronics by serving as a nondissipative circuit element. Just as semiconductor diodes are fundamental to a wide range of optical and electronic technologies, the superconducting diode opens similar avenues in superconducting electronics [3,4], superconducting spintronics [5,6], and quantum information and communication technologies [7,8]. Since the first reports on the superconducting diode effect, nonreciprocity in superconducting systems has gained a lot of attention from the experimental and theoretical sides in a multitude of systems ranging from a variety of materials with distinct underlying symmetries, diverse device geometries, and mechanisms that are believed to give rise to the nonreciprocity.

Most theoretical descriptions of the JDE predict that the simultaneous breaking of inversion and time-reversal symmetries results in a nonreciprocal Josephson current [9–17]. A lot of work has been published on the semiconductor-superconductor material platform [18–23], where this can be accomplished by the presence of spin-orbit coupling and the Rashba effect in conjunction with an external Zeeman-field for the time-reversal symmetry breaking [24–29]. The combination of both effects leads to the Cooper pairs acquiring a finite momentum, similar to Fulde-Ferrell-Larkin-Ovchinnikov states, which results in nonreciprocal critical current of the Josephson junction [14]. Alternatively, the inversion symmetry can be broken by the device layout itself. This can be achieved, for example, by a superconducting quantum interference device (SQUID), where each of the two junctions of the interferometer has a different current-phase relation [30–32]. More recently, the asymmetry in a multiterminal Josephson junction has led to a diode effect, either by keeping one of the superconducting electrodes floating [33,34] or by phase biasing using superconducting loops that connect pairs of electrodes in the junction [35]. Topological insulators, in this regard, bear an inherent advantage with respect to the presence of the diode effect. Even without the broken inversion symmetry of the bulk crystal, the topological surface states resemble Rashba-like states in a sense, in that they are spin-split and spin-momentum locked. As a result, applying an in-plane magnetic field to the surface of the topological insulator (TI) causes a unidirectional shift of the Dirac cone's Fermi surface, potentially leading to the formation of a Fulde-Ferrell-Larkin-Ovchinnikov-like states, in a sense, in that the Cooper pairs acquire a finite momentum q_0 [23,36–38]. A direct consequence of this is an intrinsic diode effect. Asymmetrical switching currents in Josephson junctions made from topological insolators and Dirac semimetals have been shown to result from such Cooper pair momentum [22,38].

*Contact author: g.behner@fz-juelich.de
†Contact author: th.schaepers@fz-juelich.de

Published by the American Physical Society under the terms of the Creative Commons Attribution 4.0 International license. Further distribution of this work must maintain attribution to the author(s) and the published article's title, journal citation, and DOI.

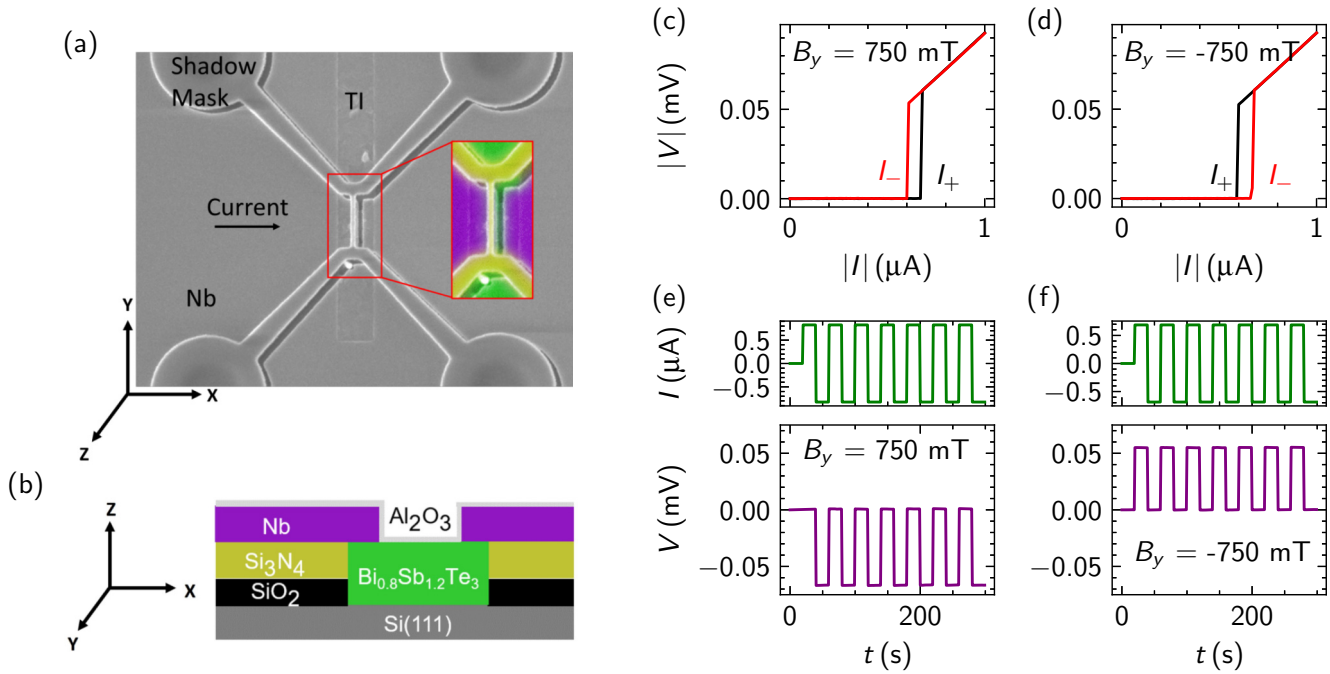

FIG. 1. Sample layout and measurement of the Josephson diode effect of junction JJ_1. (a) Scanning electron micrograph of the device, including an inset with a zoom-in on the junction area, rendered in false color for enhanced visualization. The Cartesian axes are labeled, highlighting each essential component necessary for observing the superconducting diode effect. (b) Cross section corresponding to a line cut through the junction along the transport direction. The inversion symmetry is broken in the z direction. (c) IV characteristic at an applied magnetic field B_y of 750 mT in the y direction perpendicular to transport. Here, I_+ exceeds $|I_-|$. (d) Corresponding plot at $B_y = -750$ mT, now with $|I_-|$ exceeding I_+. (e) Oscillating current of ± 600 nA at $B_y = 750$ mT and corresponding voltage drop response. The junction is in the superconducting state and the resistive state for positive and negative currents, respectively. (f) Oscillating current of ± 600 nA at $B_y = -750$ mT and corresponding voltage drop. The behavior opposite to that in panel (e) is recorded.

We present low-temperature measurements of the Josephson diode effect in junctions based on superconducting Nb electrodes bridged by the three-dimensional topological insulator $Bi_{0.8}Sb_{1.2}Te_3$. The junctions are fabricated by a combination of selective-area growth and shadow mask evaporation [39,40]. This approach allows for the *in situ* fabrication of Josephson junctions with very high interface transparency, important for the study of the superconducting proximity effect. We analyze the behavior of the junction as a function of the magnetic field, the temperature, and the microwave radiation and perform a detailed analysis of the diode effect. Two probed junctions show a pronounced diode effect. The effect is stable over multiple switching cycles and can be reversed by inverting the polarity of an in-plane magnetic field perpendicular to the current direction. Our analysis of the temperature dependence of the switching current reveals that the supercurrent is carried to a large extent by topological surface states [39,41]. In addition, the presence of half-integer Shapiro steps indicates a nonsinusoidal current-phase relationship in the junction. Based on these observations, we propose that the origin of the diode effect lies in the proximized topological surface states.

II. EXPERIMENT

The samples are fabricated by selective-area growth combined with shadow mask evaporation [39,40]. This approach allows the fabrication of samples with arbitrary geometries and excellent interface transparency between the topological insulator and the parent superconductor. First, a 10-nm-thick layer of SiO_2, followed by a 25-nm-thick layer of Si_3N_4, is deposited on a Si(111) substrate by thermal oxidation and plasma-enhanced chemical vapor deposition (PECVD), respectively, to form the selective-area growth mask. Trench widths of 400 nm are prepared using electron beam lithography and reactive ion etching (RIE). A second stack of 300-nm-thick SiO_2 and 100-nm-thick Si_3N_4 is then deposited by PECVD to form the bridge for shadow evaporation. The Si_3N_4 layer is patterned into the bridge shape by electron beam lithography and RIE. The sample is then etched with hydrofluoric acid to form a suspended bridge that acts as a shadow mask over the trench. The 18-nm-thick $Bi_{0.8}Sb_{1.2}Te_3$ topological insulator film is grown by rotating the sample around its normal axis to ensure uniform deposition under the shadow mask. Next, 50-nm-thick Nb electrodes are deposited *in situ* at an angle without rotating the sample. The shadow mask provides a gap between the two Nb electrodes, effectively patterning the Josephson junction. The junction is capped with a 5-nm-thick layer of Al_2O_3 under rotation to prevent oxidation. Finally, the electrode shape is defined *ex situ* using an SF_6 RIE process, leaving the junction area and nanoribbon unaffected. A scanning electron microscope (SEM) image is shown in Fig. 1(a), with junction details highlighted in the inset. For all measured junctions the width and the length of the weak link are 1 μm and 100 nm, respectively. The corresponding layer stack

along the x axis of the junction is shown in Fig. 1(b). The critical temperature T_c of the Nb film is determined to be approximately 8.5 K, resulting in a superconducting gap Δ of 1.3 meV [42].

The sample characteristics were measured in a dilution refrigerator with a base temperature of $T \approx 10$ mK. The differential resistance dV/dI is measured using a lock-in amplifier by adding a 10-nA AC current to the applied DC current. A vector magnet (6-1-1 T) is used to apply the magnetic field in all three Cartesian directions. The radio frequency is supplied by a standard radio-frequency source using an antenna in close vicinity to the sample.

In total, five devices, i.e., JJ_1 to JJ_5, on three separate silicon chips were studied. All junctions were equally fabricated and from the same growth run. Two out of the five junctions, i.e., JJ_1 and JJ_2 showed the Josephson diode effect. The other three samples did not show a significant diode effect, presumably because of their smaller switching current and hence an insufficient number of transport channels [24]. We attribute this to the selective-area growth approach, i.e., the different defect densities in the individually etched topological insulator trenches (see Supplemental Material [43]). The parameters of all junctions are given in the Supplemental Material [43]. In the following we discuss the Josephson diode effect of junction JJ_1, while the data of JJ_2 are given in the Supplemental Material [43].

III. RESULTS

The current-voltage (IV) characteristic of junction JJ_1 shows a hysteretic behavior. The switching current I_c and the return current I_r are measured at zero magnetic field at 10 mK and resulted in values of 0.880 and 0.360 μA, respectively (see Supplemental Material for details [43]). The normal state resistance R_N of 111 Ω is evaluated by a linear regression of the junction's Ohmic behavior at voltage biases larger than the superconducting gap 2Δ. Here, 2Δ is extracted from the critical temperature of the Nb film, $T_c \approx 8.5$ K, using $\Delta = 1.764\, k_B$ and $T_c \approx 1.3$ meV. The excess current I_{exc} of 0.945 μA is gained from the intercept of the linear regression at zero voltage. The transparency τ, as a figure of merit to evaluate the interface quality between the superconductor and the weak-link material in a Josephson junction, is obtained by fitting the analytical calculation according to the work of Niebler *et al.* [44], which is based on the Octavio-Tinkham-Blonder-Klapwijk model [45,46]. Junction JJ_1 exhibits a transparency of $\tau = 68.61\%$, which is comparable to previous similarly fabricated samples [34,41,47,48].

First, we show that junction JJ_1 indeed behaves as a Josephson diode. The performance of the Josephson diode is quantified by its rectification factor defined as $\eta = \delta I_c/(I_+ + |I_-|)$, where $\delta I_c = (I_+ - |I_-|)$. The switching currents $|I_-|$ and I_+ for negative and positive biases are measured individually by ramping the current starting at zero current. To observe the Josephson diode effect, a magnetic field B_y is applied along the y axis, i.e., perpendicular to the current direction [cf. Fig. 1(a)]. Figure 1(c) shows the current-voltage characteristics of the sample for an applied magnetic field of 750 mT. The field is directed in-plane perpendicular to the current direction. For positive field, $I_+ = 660$ nA exceeds $|I_-| = 589$ nA, yielding a diode rectification factor of about $\eta \approx 5.5\,\%$. When switching the magnetic field direction the diode effect inverts. This can be seen in Fig. 1(d), which depicts the IV characteristics under application of $B_y = -750$ mT. Now, $|I_-|$ exceeds I_+, yielding $\eta \approx -5.6\%$. In order to demonstrate the switching between superconductive and resistive state, the bias current is varied between ±600 nA, i.e., a current magnitude between the two switching currents, while the voltage drop is recorded. This is shown in Figs. 1(e) and 1(f) for both field set points, respectively. For $B_y = 750$ mT, the junction is in the superconducting state for a positive bias current but in the resistive state for a negative bias current. At the opposite field $B_y = -750$ mT, this behavior switches, and the junction is in the superconducting state for a negative bias current but in the resistive state for a positive bias current. Next, we analyze the evolution of the Josephson diode effect over the whole range of magnetic fields in the B_x-B_y plane. The diode effect occurs when the axes of current flow, inversion symmetry, and time-reversal symmetry are perpendicular to each other. [18]. As the inversion symmetry is broken by the device layout in the z direction, and current flow takes place in the x direction, we expect diode behavior only for fields applied in the B_y direction. Figure 2(a) shows the evolution of I_- and I_+ of junction JJ_1 as a function of the applied magnetic field B_y in the y direction. The magnetic field is swept over a range of ±1 T with the absolute values of the switching current decreasing only by a factor of about 2. This is consistent for all measured junctions and is attributed to the direction of the magnetic field with respect to the junction, i.e., the small cross section given by the thickness of the topological insulator nanoribbon and the junction length, penetrated by the magnetic field [49,50]. One finds that a finite diode effect develops already for fields larger than 100 mT. The sign of the diode effect switches with inverting the magnetic field direction. As a statistical spread of the switching current was noticed at zero field, a statistical analysis of the effect is carried out. For each point in the plot, the corresponding IV characteristics are measured five times each, averaged, and plotted with the corresponding error bars. A full analysis of the statistical spread of the switching current at selected magnetic fields along the x and y axes is given in the Supplemental Material [43]. One finds that the size of the effect is larger than the spread of the error on the switching current. In Fig. 2(b), the diode rectification factor η is plotted as a function of the magnetic field B_y. The maximum diode rectification factor is determined to be $\eta_{max} = 7\%$.

Theoretical work has been conducted on the Josephson diode effect in topological insulators, as well as in Rashba superconductors. These studies predict rectification factors of 20% and 40% and indicate that rectification in these systems depends significantly on factors such as magnetic field, gate voltage, and junction length [15,23]. In other materials with strong spin-orbit coupling, rectification factors have been experimentally determined to range from 2% to as high as 60% in exfoliated $NbTe_2$ crystals and InSb-, InAs-, and $NbSe_2$-based Josephson junctions [18,19,22,51]. As outlined in detail below, we attribute the deviation of the rectification factor of our junction from the theoretically predicted values to the presence of parallel ballistic and diffusive channels, where only the ballistic channels meet the criteria necessary

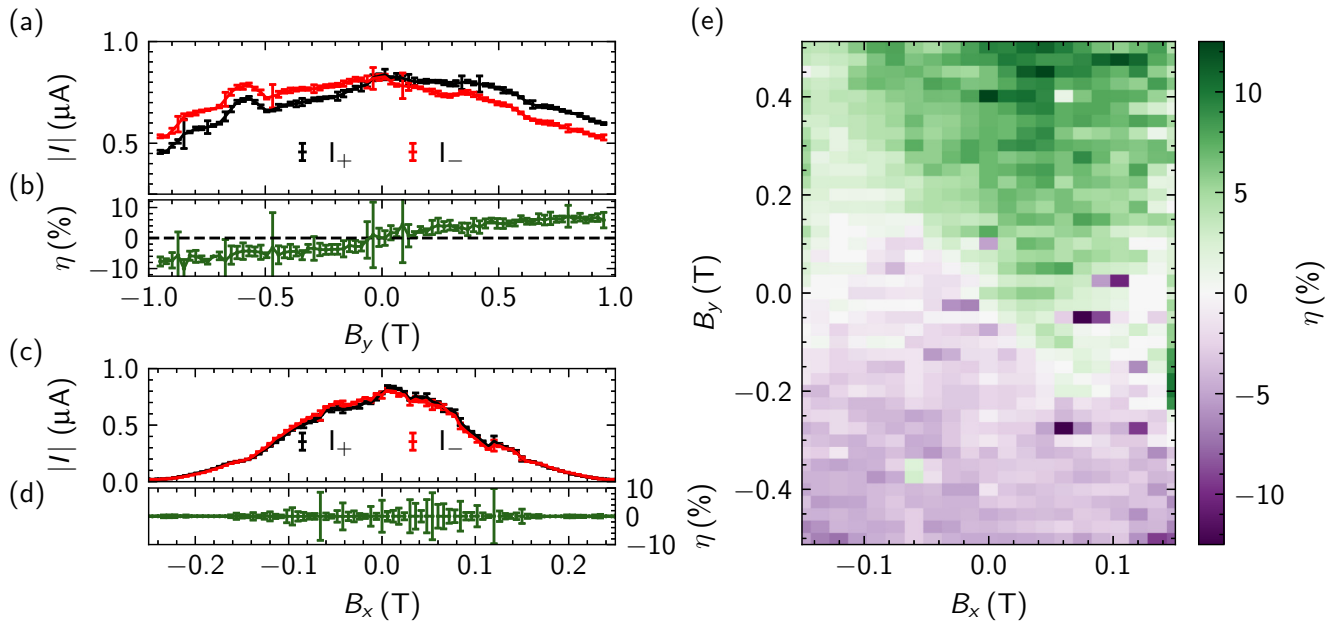

FIG. 2. Full analysis of the Josephson diode effect in JJ_1 under application of magnetic fields in the x-y plane. (a) Switching currents $|I_-|$ and I_+ as a function of applied fields in the y direction, i.e., perpendicular to transport. (b) Diode rectification factor η as a function of a magnetic field applied in the y direction. The errors for η are determined using standard error propagation rules. (c) Switching currents $|I_-|$ and I_+ as a function of applied fields in the x direction, parallel to transport. The switching current diminishes to zero for fields larger than 250 mT. No Josephson diode effect is present. (d) Diode rectification factor η as a function of a magnetic field applied in the x direction. (e) Map of the diode rectification factor η as a function of B_x and B_y.

for generating a nonreciprocal supercurrent. The existence of parallel channels can be deduced from the temperature-dependent critical current, which is analyzed in the following sections. Especially for higher fields, the statistical spread shrinks and a stable diode effect is recorded. Figure 2(c) shows the switching currents $|I_-|$ and I_+ of JJ_1 as a function of the magnetic field applied in the x direction. The switching currents decrease to zero over a span of 250 mT. As can be seen from the value of the rectification factor, shown in Fig. 2(d), there is no significant diode effect when the magnetic field is aligned with the current direction. A map of the rectification factor, shown in Fig. 2(e), provides a complete picture of how it varies with B_x and B_y. Clearly, the diode effect occurs primarily when magnetic fields are applied along the y direction. Magnetic fields in the x direction have only a minor effect on the rectification factor. An additional in-plane component may affect the superconducting diode effect due to asymmetric spin-orbit coupling, as observed in related magnetochiral anisotropy effects measured in T_d-$MoTe_2$ [52] Previous studies have reported on magnetochiral anisotropy in topological insulators and Rashba materials [53–55] and have theoretically explored the superconducting diode effect in these material systems [56,57]. Since the axis of symmetry breaking is typically perpendicular to the layer, one would expect the diode effect to occur with in-plane magnetic fields perpendicular to the current. However, deviations are possible due to inhomogeneities in the layers, such as variations in layer thickness or defects.

In Fig. 3, the switching currents $|I_-|$ and I_+ are given as a function of temperature at an applied in-plane field of $B_y = 750$ mT. It can be seen that the diode effect is present up to temperatures of about 400 mK. This is consistent with observations that higher harmonic terms in the current-phase relationship disappear with increasing temperature [19].

Indeed, in order to exhibit a diode effect, the samples have to have a large number of transport channels [24]. We therefore attribute the fact that only junctions JJ_1 and JJ_2 show the diode effect to the presence of a sufficiently large number of transport channels. According to the theoretical models, a nonsinusoidal current-phase relationship is required for a weak-link junction to exhibit an Josephson diode effect [14,24–29]. Indeed, using an asymmetric superconducting quantum interference device, a highly skewed current-phase relationship was measured for a topological insulator weak link, which was attributed to quasiballistic transport in the topological surface states [58]. In order to identify the con-

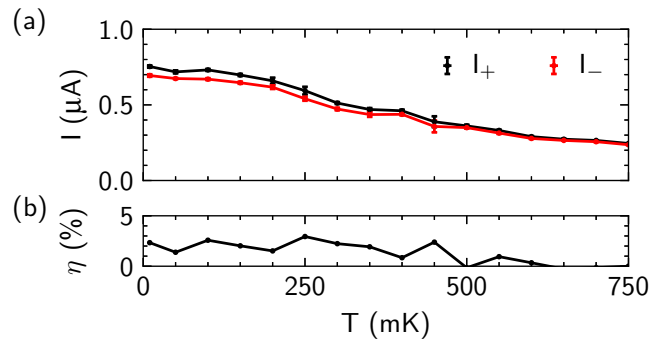

FIG. 3. (a) Switching currents $|I_-|$ and I_+ at $B_y = 750$ mT as a function of temperature. (b) Corresponding diode rectification factor η as a function of temperature.

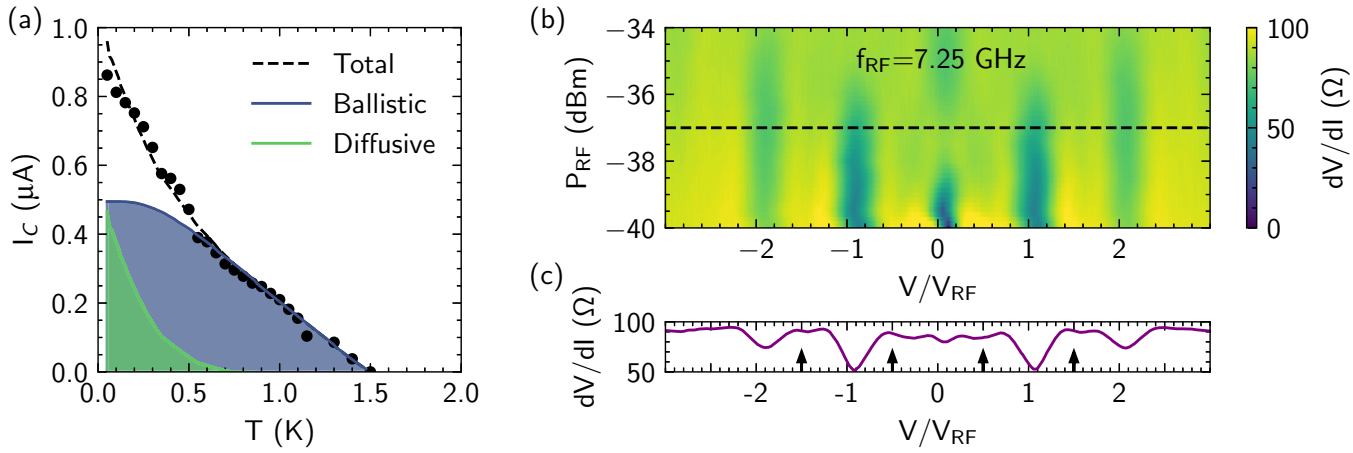

FIG. 4. (a) Temperature dependence of the switching current of junction JJ_1. The dashed black line shows the calculated switching current. It consists of ballistic (blue) and diffusive (green) contributions. (b) Differential resistance dV/dI as a function of the applied microwave power P_{RF} and the DC voltage normalized by the characteristic voltage $V_{RF} = hf_{RF}/2e$. Vertical lines in the color map correspond to dips in the differential voltage of the sample associated with plateaus in the IV characteristics of the junctions. Dips are observed at integer positions of V_{RF}. In addition, slightly less pronounced dips can be seen at half integer values of V_{RF}. (c) Line cut of panel (b) at $P_{RF} = -37$ dBm. Arrows in the plot indicate the position of the fractional Shapiro steps at $n = \pm 0.5$ and ± 1.5.

tributing transport channels for our samples, we measured the temperature dependence of the switching current for JJ_1 [see Fig. 4(a)]. We used the clean-limit Eilenberger equations to model the ballistic component of the surface states [59,60], while the Usadel equations were employed for the diffusive component [61]. Following the reasoning given by Schüffelgen *et al.* [39] and Schmitt *et al.* [41], the switching current is given by a diffusive and ballistic contribution, with the diffusive contribution diminishing at around 0.7 K. Beyond that value, the supercurrent is only carried by the ballistic channel. The existence of a ballistic surface channel was also deduced from temperature-dependent Aharonov-Bohm effect measurements on topological insulator ring structures [62].

At low temperatures, weak-link junctions containing a ballistic contribution should exhibit a nonsinusoidal current-phase relationship [63]. In order to check for this, we have recorded the IV characteristics of our junctions under microwave radiation to detect Shapiro steps. For these measurements, the presence of half-integer Shapiro steps in addition to integer steps is considered as a signature of a nonsinusoidal current-phase relationship [64–67]. Figure 4(b) shows the differential resistance dV/dI of junction JJ_1 as a function of the applied microwave power P_{RF} and the normalized measured voltage drop V/V_{RF}, where $V_{RF} = hf_{RF}/2e$ with f_{RF} being the radio-frequency (RF) frequency, h the Planck constant, and e the electron charge. Shapiro steps in the IV characteristics are expected to appear at voltages $V = nV_{RF}$, with n being an integer number. These steps correspond to dips at integer values of V/V_{RF} in the differential resistance, which are indeed found in Fig. 4(b) at $n = 0$, ± 1, and ± 2. In addition, less pronounced dips can be seen in between at $n = \pm 0.5$ and ± 1.5, corresponding to half-integer Shapiro steps. To emphasize their visibility, a line cut at -37 dBm is plotted in Fig. 4(c) showing dV/dI as a function of V/V_{RF}. The dips at $n = \pm 0.5$ and ± 1.5 are marked with vertical arrows. Together with the temperature-dependent measurements, showing a ballistic switching current contribution, we can conclude that the current-phase relation is nonsinusoidal, which is an essential prerequisite for the occurrence of the Josephson diode effect.

Taking into account the results of the temperature-dependent measurements and the measurements under microwave irradiation, we come to the following conclusions for the presence of the diode effect in our Josephson junctions. The temperature dependence of the switching current indicates the presence of a ballistic contribution to the switching current. We attribute this contribution to the existence of proximitized surface states in our junction [39,41]. As mentioned above, the presence of ballistic modes due to the topological surface states is also confirmed by measurements of the Aharonov-Bohm effect on ring structures [62]. It is therefore plausible to assume that our junctions reside in the short ballistic junction limit since the junction length $L \approx 100$ nm is much shorter than the coherence length of charger carriers in the material system at the present temperatures [62]. This results in a nonsinusoidal, i.e., a skewed, current-phase relation [63,68,69]. Indeed, from the appearance of half-integer Shapiro steps we can conclude that our junctions have a nonsinusoidal current-phase relation [64–67]. For topological insulator based junctions, a skewed current-phase relation has also been confirmed by an alternative measurement scheme using an asymmetric SQUID structure [58,70]. The accidental formation of a SQUID in our junction, which could potentially lead to a nonsinusoidal current-phase relationship, can be excluded based on the Fraunhofer pattern presented in the Supplemental Material [43]. A nonsinusoidal current-phase relationship is a necessary component for the presence of the superconducting diode effect [18]; however, it is not sufficient on its own to achieve a Josephson diode effect. In addition, an anomalous phase shift is required. This phase shift results from the finite-momentum Cooper pairing induced by the shift of the Fermi contours, as a result of the applied in-plane field [14,23,36–38], and has been observed in Bi_2Se_3-based Josephson junctions when an in-plane mag-

netic field is applied [38,71]. For junctions in the ballistic regime, this leads to an anomalous current-phase relation whose Fourier expansion includes both cosine and sinusoidal terms. As a result, not only a simple phase shift is observed but also a difference in the positive and negative current branches of the current-phase relation, i.e., a Josephson diode effect.

IV. CONCLUSION

In conclusion, we have demonstrated that $Nb/Bi_{0.8}Sb_{1.2}Te_3/Nb$ Josephson junctions made of selectively grown topological insulator weak links can exhibit nonreciprocal charge transport in the superconducting regime under the application of an in-plane magnetic field perpendicular to the transport. The superconducting diode effect has been studied in the whole range of in-plane magnetic fields, and these measurements confirm that the diode effect is present when the magnetic field is oriented perpendicular to the current direction. Based on temperature-dependent measurements of the switching current, we conclude that the origin of the effect is the proximization of spin-orbit-coupled ballistic surface states, which experience a Zeeman shift due to the applied magnetic field. With the presence of fractional Shapiro steps, the junctions also provide evidence for the existence of a nonsinusoidal current-phase relationship, necessary for the Josephson diode effect. So far, the superconducting diode effect in topological insulators has been studied only to a limited extent. However, since it seems to be the result of proximized topological surface states, it expands the toolbox of experiments that can be used in the ongoing research on topological Josephson junctions. As a future perspective, theoretical studies suggest that the 4π-periodic contribution of Majorana fermions to the current-phase relation in a Josephson junction could lead to a significant enhancement of the diode effect [72,73]. Further studies may leverage this phenomenon to detect topological phase transitions in topological insulator based Josephson junctions under applied magnetic fields.

ACKNOWLEDGMENTS

We thank H. Kertz for technical assistance, and F. Lentz and S. Trellenkamp for electron beam lithography. We are grateful for fruitful discussions with K. Moors and T. Wakamura. This work was partly funded by the Deutsche Forschungsgemeinschaft (DFG, German Research Foundation) under Germany's Excellence Strategy, Cluster of Excellence Matter and Light for Quantum Computing (ML4Q), Grant No. EXC 2004/1–390534769, and was financially supported by the Bavarian Ministry of Economic Affairs, Regional Development and Energy within Bavaria's High-Tech Agenda Project "Bausteine für das Quantencomputing auf Basis Topologischer Materialien mit Experimentellen und Theoretischen Ansätzen" (Grant No. 07 02/686 58/1/21 1/22 2/23). Furthermore, this work is supported by the QuantERA grant MAGMA and by the Deutsche Forschungsgemeinschaft (DFG, German Research Foundation) under Grant No. 491798118. G.B. thanks NTT Basic Research Laboratories for the hospitality during his research stay.

DATA AVAILABILITY

The data that support the findings of this article are openly available [1], embargo periods may apply.

[1] M. Nadeem, M. S. Fuhrer, and X. Wang, The superconducting diode effect, Nat. Rev. Phys. **5**, 558 (2023).
[2] J. Ma, R. Zhan, and X. Lin, Superconducting diode effects: Mechanisms, materials and applications, Adv. Phys. Res. **4**, 2400180 (2025).
[3] A. I. Braginski, Superconductor electronics: Status and outlook, J. Supercond. Novel Magn. **32**, 23 (2018).
[4] R. Bairamkulov and G. De Micheli, Superconductive electronics: A 25-year review [feature], IEEE Circuits Syst. Mag. **24**, 16 (2024).
[5] J. Linder and J. W. A. Robinson, Superconducting spintronics, Nat. Phys. **11**, 307 (2015).
[6] R. Cai, I. Žutić, and W. Han, Superconductor/ferromagnet heterostructures: A platform for superconducting spintronics and quantum computation, Adv. Quantum Technol. **6**, 2200080 (2022).
[7] G. Wendin, Quantum information processing with superconducting circuits: A review, Rep. Prog. Phys. **80**, 106001 (2017).
[8] X. Liu and M. C. Hersam, 2D materials for quantum information science, Nat. Rev. Mater. **4**, 669 (2019).
[9] M. Davydova, S. Prembabu, and L. Fu, Universal Josephson diode effect, Sci. Adv. **8**, eabo0309 (2022).
[10] K. Misaki and N. Nagaosa, Theory of the nonreciprocal Josephson effect, Phys. Rev. B **103**, 245302 (2021).
[11] Y. Zhang, Y. Gu, P. Li, J. Hu, and K. Jiang, General theory of Josephson diodes, Phys. Rev. X **12**, 041013 (2022).
[12] Y. Tanaka, B. Lu, and N. Nagaosa, Theory of giant diode effect in d-wave superconductor junctions on the surface of a topological insulator, Phys. Rev. B **106**, 214524 (2022).
[13] A. Daido, Y. Ikeda, and Y. Yanase, Intrinsic superconducting diode effect, Phys. Rev. Lett. **128**, 037001 (2022).
[14] N. F. Q. Yuan and L. Fu, Supercurrent diode effect and finite-momentum superconductors, Proc. Natl. Acad. Sci. USA **119**, e2119548119 (2022).
[15] S. Ilić and F. S. Bergeret, Theory of the supercurrent diode effect in Rashba superconductors with arbitrary disorder, Phys. Rev. Lett. **128**, 177001 (2022).
[16] T. Karabassov, I. V. Bobkova, A. A. Golubov, and A. S. Vasenko, Hybrid helical state and superconducting diode effect in superconductor/ferromagnet/topological insulator heterostructures, Phys. Rev. B **106**, 224509 (2022).
[17] B. Zinkl, K. Hamamoto, and M. Sigrist, Symmetry conditions for the superconducting diode effect in chiral superconductors, Phys. Rev. Res. **4**, 033167 (2022).
[18] C. Baumgartner, L. Fuchs, A. Costa, S. Reinhardt, S. Gronin, G. C. Gardner, T. Lindemann, M. J. Manfra, P. E. Faria Junior, D. Kochan, *et al.*, Supercurrent rectification and magnetochiral effects in symmetric Josephson junctions, Nat. Nanotechnol. **17**, 39 (2022).

[19] B. Turini, S. Salimian, M. Carrega, A. Iorio, E. Strambini, F. Giazotto, V. Zannier, L. Sorba, and S. Heun, Josephson diode effect in high-mobility InSb nanoflags, Nano Lett. **22**, 8502 (2022), .

[20] A. Costa, C. Baumgartner, S. Reinhardt, J. Berger, S. Gronin, G. Gardner, T. Lindemann, M. Manfra, J. Fabian, D. Kochan, *et al.*, Sign reversal of the Josephson inductance magnetochiral anisotropy and 0–π-like transitions in supercurrent diodes, Nat. Nanotechnol. **18**, 1266 (2023).

[21] N. Lotfizadeh, W. F. Schiela, B. Pekerten, P. Yu, B. H. Elfeky, W. M. Strickland, A. Matos-Abiague, and J. Shabani, Superconducting diode effect sign change in epitaxial Al-InAs Josephson junctions, Commun. Phys. **7**, 120 (2024).

[22] B. Pal, A. Chakraborty, P. K. Sivakumar, M. Davydova, A. K. Gopi, A. K. Pandeya, J. A. Krieger, Y. Zhang, M. Date, S. Ju, *et al.*, Josephson diode effect from Cooper pair momentum in a topological semimetal, Nat. Phys. **18**, 1228 (2022).

[23] B. Lu, S. Ikegaya, P. Burset, Y. Tanaka, and N. Nagaosa, Tunable Josephson diode effect on the surface of topological insulators, Phys. Rev. Lett. **131**, 096001 (2023).

[24] A. A. Reynoso, G. Usaj, C. A. Balseiro, D. Feinberg, and M. Avignon, Spin-orbit-induced chirality of Andreev states in Josephson junctions, Phys. Rev. B **86**, 214519 (2012).

[25] T. Yokoyama, M. Eto, and Y. V. Nazarov, Josephson current through semiconductor nanowire with spin–orbit interaction in magnetic field, J. Phys. Soc. Jpn. **82**, 054703 (2013).

[26] T. Yokoyama, M. Eto, and Y. V. Nazarov, Anomalous Josephson effect induced by spin-orbit interaction and Zeeman effect in semiconductor nanowires, Phys. Rev. B **89**, 195407 (2014).

[27] F. Dolcini, M. Houzet, and J. S. Meyer, Topological Josephson ϕ_0 junctions, Phys. Rev. B **92**, 035428 (2015).

[28] Z. Liu, L. Huang, and J. Wang, Josephson diode effect in topological superconductors, Phys. Rev. B **110**, 014519 (2024).

[29] J. S. Meyer and M. Houzet, Josephson diode effect in a ballistic single-channel nanowire, Appl. Phys. Lett. **125**, 022603 (2024).

[30] R. S. Souto, M. Leijnse, and C. Schrade, Josephson diode effect in supercurrent interferometers, Phys. Rev. Lett. **129**, 267702 (2022).

[31] E. Nikodem, J. Schluck, M. Geier, M. Papaj, H. F. Legg, J. Feng, M. Bagchi, L. Fu, and Y. Ando, Tunable superconducting diode effect in a topological nano-SQUID, Sci. Adv. **11**, eadw4898 (2025).

[32] Y. V. Fominov and D. S. Mikhailov, Asymmetric higher-harmonic SQUID as a Josephson diode, Phys. Rev. B **106**, 134514 (2022).

[33] M. Gupta, G. V. Graziano, M. Pendharkar, J. T. Dong, C. P. Dempsey, C. Palmström, and V. S. Pribiag, Gate-tunable superconducting diode effect in a three-terminal Josephson device, Nat. Commun. **14**, 3078 (2023).

[34] G. Behner, A. R. Jalil, A. Rupp, H. Lüth, D. Grützmacher, and T. Schäpers, Superconductive coupling effects in selectively grown topological insulator-based three-terminal junctions, ACS Nano **19**, 3878 (2025).

[35] M. Coraiola, A. E. Svetogorov, D. Z. Haxell, D. Sabonis, M. Hinderling, S. C. ten Kate, E. Cheah, F. Krizek, R. Schott, W. Wegscheider, J. C. Cuevas, W. Belzig, and F. Nichele, Flux-tunable Josephson diode effect in a hybrid four-terminal Josephson junction, ACS Nano **18**, 9221 (2024).

[36] Z. Zheng, M. Gong, Y. Zhang, X. Zou, C. Zhang, and G. Guo, FFLO superfluids in 2D spin-orbit coupled Fermi gases, Sci. Rep. **4**, 6535 (2014).

[37] M. J. Park, J. Yang, Y. Kim, and M. J. Gilbert, Fulde-Ferrell states in inverse proximity-coupled magnetically doped topological heterostructures, Phys. Rev. B **96**, 064518 (2017).

[38] A. Q. Chen, M. J. Park, S. T. Gill, Y. Xiao, D. Reig-i Plessis, G. J. MacDougall, M. J. Gilbert, and N. Mason, Finite momentum Cooper pairing in three-dimensional topological insulator Josephson junctions, Nat. Commun. **9**, 3478 (2018).

[39] P. Schüffelgen, D. Rosenbach, C. Li, T. W. Schmitt, M. Schleenvoigt, A. R. Jalil, S. Schmitt, J. Kölzer, M. Wang, B. Bennemann, U. Parlak, L. Kibkalo, S. Trellenkamp, T. Grap, D. Meertens, M. Luysberg, G. Mussler, E. Berenschot, N. Tas, A. A. Golubov, *et al.*, Selective area growth and stencil lithography for *in situ* fabricated quantum devices, Nat. Nanotechnol. **14**, 825 (2019).

[40] A. R. Jalil, P. Schüffelgen, H. Valencia, M. Schleenvoigt, C. Ringkamp, G. Mussler, M. Luysberg, J. Mayer, and D. Grützmacher, Selective area epitaxy of quasi-1-dimensional topological nanostructures and networks, Nanomaterials **13**, 354 (2023).

[41] T. W. Schmitt, B. Frohn, W. Wittl, A. R. Jalil, M. Schleenvoigt, E. Zimmermann, A. Schmidt, T. Schäpers, J. C. Cuevas, A. Brinkman, D. Grützmacher, and P. Schüffelgen, Anomalous temperature dependence of multiple Andreev reflections in a topological insulator Josephson junction, Supercond. Sci. Technol. **36**, 024002 (2023).

[42] J. P. Carbotte, Properties of boson-exchange superconductors, Rev. Mod. Phys. **62**, 1027 (1990).

[43] See Supplemental Material at http://link.aps.org/supplemental/10.1103/gc7k-rn8q for additional measurements of JJ1 and for a second dataset obtained from a similar device (JJ2) on another chip, which also includes Refs. [18,21,24,34,39,41,47,59–61,74–79].

[44] G. Niebler, G. Cuniberti, and T. Novotný, Analytical calculation of the excess current in the Octavio–Tinkham–Blonder–Klapwijk theory, Supercond. Sci. Technol. **22**, 085016 (2009).

[45] M. Octavio, M. Tinkham, G. E. Blonder, and T. M. Klapwijk, Subharmonic energy-gap structure in superconducting constrictions, Phys. Rev. B **27**, 6739 (1983).

[46] K. Flensberg, J. B. Hansen, and M. Octavio, Subharmonic energy-gap structure in superconducting weak links, Phys. Rev. B **38**, 8707 (1988).

[47] D. Rosenbach, A. R. Jalil, T. W. Schmitt, B. Bennemann, G. Mussler, P. Schüffelgen, D. Grützmacher, and T. Schäpers, Ballistic surface channels in fully *in situ* defined Bi_4Te_3 Josephson junctions with aluminum contacts, arXiv:2301.03968.

[48] A. R. Jalil, T. W. Schmitt, P. Rüßmann, X. Wei, B. Frohn, M. Schleenvoigt, W. Wittl, X. Hou, A. Schmidt, K. Underwood, G. Bihlmayer, M. Luysberg, J. Mayer, S. Blügel, D. Grützmacher, and P. Schüffelgen, Engineering epitaxial interfaces for topological insulator — superconductor hybrid devices with Al electrodes, Adv. Quantum Technol. **8**, 2400343 (2024).

[49] J. C. Cuevas and F. S. Bergeret, Magnetic interference patterns and vortices in diffusive SNS junctions, Phys. Rev. Lett. **99**, 217002 (2007).

[50] H. Y. Günel, I. E. Batov, H. Hardtdegen, K. Sladek, A. Winden, K. Weis, G. Panaitov, D. Grützmacher, and T. Schäpers,

Supercurrent in Nb/InAs-nanowire/Nb Josephson junctions, J. Appl. Phys. **112**, 034316 (2012).

[51] L. Bauriedl, C. Bäuml, L. Fuchs, C. Baumgartner, N. Paulik, J. M. Bauer, K.-Q. Lin, J. M. Lupton, T. Taniguchi, K. Watanabe, C. Strunk, and N. Paradiso, Supercurrent diode effect and magnetochiral anisotropy in few-layer $NbSe_2$, Nat. Commun. **13**, 4266 (2022).

[52] W.-S. Du, W. Chen, Y. Zhou, T. Zhou, G. Liu, Z. Xiao, Z. Zhang, Z. Miao, H. Jia, S. Liu, Y. Zhao, Z. Zhang, T. Chen, N. Wang, W. Huang, Z.-B. Tan, J.-J. Chen, and D.-P. Yu, Superconducting diode effect and large magnetochiral anisotropy in T_d-$MoTe_2$ thin film, Phys. Rev. B **110**, 174509 (2024).

[53] T. Ideue, K. Hamamoto, S. Koshikawa, M. Ezawa, S. Shimizu, Y. Kaneko, Y. Tokura, N. Nagaosa, and Y. Iwasa, Bulk rectification effect in a polar semiconductor, Nat. Phys. **13**, 578 (2017).

[54] D. C. Marinescu and S. Tewari, Magnetochiral anisotropy induced nonlinear planar Hall effect in topological insulator surface states, Phys. Rev. B **109**, 205301 (2024).

[55] H. F. Legg, M. Rößler, F. Münning, D. Fan, O. Breunig, A. Bliesener, G. Lippertz, A. Uday, A. Taskin, D. Loss, *et al.*, Giant magnetochiral anisotropy from quantum-confined surface states of topological insulator nanowires, Nat. Nanotechnol. **17**, 696 (2022).

[56] J. J. He, Y. Tanaka, and N. Nagaosa, A phenomenological theory of superconductor diodes, New J. Phys. **24**, 053014 (2022).

[57] H. F. Legg, D. Loss, and J. Klinovaja, Superconducting diode effect due to magnetochiral anisotropy in topological insulators and Rashba nanowires, Phys. Rev. B **106**, 104501 (2022).

[58] M. Kayyalha, A. Kazakov, I. Miotkowski, S. Khlebnikov, L. P. Rokhinson, and Y. P. Chen, Highly skewed current–phase relation in superconductor–topological insulator–superconductor Josephson junctions, npj Quantum Mater. **5**, 7 (2020).

[59] G. Eilenberger, Transformation of Gorkov's equation for type II superconductors into transport-like equations, Z. Phys. A **214**, 195 (1968).

[60] A. V. Galaktionov and A. D. Zaikin, Quantum interference and supercurrent in multiple-barrier proximity structures, Phys. Rev. B **65**, 184507 (2002).

[61] K. D. Usadel, Generalized diffusion equation for superconducting alloys, Phys. Rev. Lett. **25**, 507 (1970).

[62] G. Behner, A. R. Jalil, D. Heffels, J. Kölzer, K. Moors, J. Mertens, E. Zimmermann, G. Mussler, P. Schüffelgen, H. Lüth, D. Grützmacher, and T. Schäpers, Aharonov-Bohm interference and phase-coherent surface-state transport in topological insulator rings, Nano Lett. **23**, 6347 (2023).

[63] A. A. Golubov, M. Y. Kupriyanov, and E. Il'ichev, The current-phase relation in Josephson junctions, Rev. Mod. Phys. **76**, 411 (2004).

[64] R. A. Snyder, C. J. Trimble, C. C. Rong, P. A. Folkes, P. J. Taylor, and J. R. Williams, Weak-link Josephson junctions made from topological crystalline insulators, Phys. Rev. Lett. **121**, 097701 (2018).

[65] B. Raes, N. Tubsrinuan, R. Sreedhar, D. S. Guala, R. Panghotra, H. Dausy, C. C. de Souza Silva, and J. Van de Vondel, Fractional Shapiro steps in resistively shunted Josephson junctions as a fingerprint of a skewed current-phase relationship, Phys. Rev. B **102**, 054507 (2020).

[66] J. Kölzer, A. R. Jalil, D. Rosenbach, L. Arndt, G. Mussler, P. Schüffelgen, D. Grützmacher, H. Lüth, and T. Schäpers, Supercurrent in Bi_4Te_3 topological material-based three-terminal junctions, Nanomaterials **13**, 293 (2023).

[67] A. Iorio, A. Crippa, B. Turini, S. Salimian, M. Carrega, L. Chirolli, V. Zannier, L. Sorba, E. Strambini, F. Giazotto, and S. Heun, Half-integer Shapiro steps in highly transmissive InSb nanoflag Josephson junctions, Phys. Rev. Res. **5**, 033015 (2023).

[68] T. Schäpers, *Superconductor/Semiconductor Junctions*, Springer Tracts in Modern Physics, Vol. 174 (Springer-Verlag, Berlin, 2001).

[69] A. Murani, Superconducting proximity effect in monocrystalline bismuth nanowires, Ph.D. thesis, Université Paris Saclay, 2017, https://theses.hal.science/tel-02057273v1.

[70] A. P. Surendran, D. Montemurro, G. Kunakova, X. Palermo, K. Niherysh, E. Trabaldo, D. S. Golubev, J. Andzane, D. Erts, F. Lombardi, and T. Bauch, Current-phase relation of a short multi-mode Bi_2Se_3 topological insulator nanoribbon Josephson junction with ballistic transport modes, Supercond. Sci. Technol. **36**, 064003 (2023).

[71] A. Assouline, C. Feuillet-Palma, N. Bergeal, T. Zhang, A. Mottaghizadeh, A. Zimmers, E. Lhuillier, M. Eddrie, P. Atkinson, M. Aprili, and H. Aubin, Spin-orbit induced phase-shift in Bi_2Se_3 Josephson junctions, Nat. Commun. **10**, 126 (2019).

[72] H. F. Legg, K. Laubscher, D. Loss, and J. Klinovaja, Parity-protected superconducting diode effect in topological Josephson junctions, Phys. Rev. B **108**, 214520 (2023).

[73] J. Cayao, N. Nagaosa, and Y. Tanaka, Enhancing the Josephson diode effect with Majorana bound states, Phys. Rev. B **109**, L081405 (2024).

[74] H. Courtois, M. Meschke, J. T. Peltonen, and J. P. Pekola, Origin of hysteresis in a proximity Josephson junction, Phys. Rev. Lett. **101**, 067002 (2008).

[75] T. A. Fulton and L. N. Dunkleberger, Lifetime of the zero-voltage state in Josephson tunnel junctions, Phys. Rev. B **9**, 4760 (1974).

[76] D. Massarotti, L. Longobardi, L. Galletti, D. Stornaiuolo, D. Montemurro, G. Pepe, G. Rotoli, A. Barone, and F. Tafuri, Escape dynamics in moderately damped Josephson junctions (review article), Low Temp. Phys. **38**, 263 (2012).

[77] J. A. Blackburn, M. Cirillo, and N. Grønbech-Jensen, Investigation of low temperature quantum crossover in Josephson junctions, J. Appl. Phys. **122**, 133904 (2017).

[78] T. F. Q. Larson, L. Zhao, E. G. Arnault, M.-T. Wei, A. Seredinski, H. Li, K. Watanabe, T. Taniguchi, F. Amet, and G. Finkelstein, Zero crossing steps and anomalous Shapiro maps in graphene Josephson junctions, Nano Lett. **20**, 6998 (2020).

[79] D. Margineda, A. Crippa, E. Strambini, Y. Fukaya, M. T. Mercaldo, M. Cuoco, and F. Giazotto, Sign reversal diode effect in superconducting Dayem nanobridges, Commun. Phys. **6**, 343 (2023).